Response to Reviewer #2

This manuscript examines the impact of horizontal resolution on ENSO amplitude in the FGOALS-f3 model. The authors show that differences in the meridional structure of zonal wind stress anomalies lead to changes in thermocline and zonal advective feedbacks within the BJ framework, thereby modulating ENSO amplitude and regularity.

Overall, the manuscript is well-organized and mostly clear. The conclusions drawn from the analysis are generally sound and suggest important implications. However, further refinements in the presentation and result interpretation would significantly enhance its overall impact and persuasiveness. Please see the following comments:

We thank the reviewer for his/her valuable and insightful comments and suggestions that help improve the manuscript. Following are the point-to-point replies to the comments (blue indicates original comment, and black indicates our reply).

1. The manuscript contains numerous equations and symbolic representations. It would improve clarity if the notation were made more consistent throughout the paper. For example, overbars and primes are both used to denote anomalies in different places, and in some places, primes seem to indicate filtered anomalies. A clearer and more unified notation system would help readers follow the derivations more easily.

Reply: We thank the reviewer for this valuable suggestion. We agree that the notation in the previous manuscript was not sufficiently unified, particularly regarding the meanings of overbars, primes, and filtered anomalies.

In the revised manuscript, we have carefully standardized the notation throughout the paper as follows:

(1) Overbars consistently denote the climatological mean (or basic-state) quantities;

(2) Primes consistently denote the interannual anomalies obtained by removing the climatological seasonal cycle.

(3) For the high-frequency (HF) wind diagnostics, we now explicitly use the subscript 'HF' to denote the HF-filtered anomalies (e.g., u'_{HF}), so as to distinguish them from the interannual anomalies used in the BJ index framework.

In addition, we have revised the text in the Methods section to define these notations explicitly when they first appear, and we have checked the equations and surrounding descriptions throughout the manuscript to ensure consistency.

For the reviewer's convenience, some notations are copied below.

"*Throughout this study, an overbar* $\overline{()}$ *denotes the climatological mean field, and*

a prime ( )' denotes the interannual anomaly obtained by removing the climatological seasonal cycle. The subscript 'HF' indicates the HF (sub-90-day) filtered field. For example, u'_{HF} denotes the HF component of daily zonal wind anomaly, obtained by applying a 90-day high-pass filter to the daily anomaly field. All symbols are used consistently throughout the paper unless otherwise specified."

We believe these revisions have substantially improved the clarity and readability of the manuscript.

2. The BJ index calculation assumes a fixed mixed layer depth of 65 m. Since model resolution may affect vertical stratification and mixed layer structure, it would be helpful if the authors could discuss the potential sensitivity of their results to this assumption. For example, would the use of model-specific mixed layer depths change the quantitative estimates of the feedback components?

Reply: We thank the reviewer for this insightful comment. As suggested, we have examined the sensitivity of the BJ index results to the mixed layer depth (MLD) assumption.

We first examined the spatial distribution of the climatological MLD in f3-L and f3-H. Here the MLD is defined as the depth at which the ocean temperature is 0.8ºC lower than the SST, following Wang et al. (2012) and Chen et al. (2016). As shown in Figure B1, the climatological MLD exhibits a pronounced zonal variation along the equatorial Pacific: it is relatively shallow in the far eastern Pacific and gradually deepens toward the central equatorial Pacific. Moreover, the MLD differs between the two model versions, with the eastern box-mean value of approximately 65 m in f3-L and 50 m in f3-H over the eastern equatorial Pacific (i.e., the BJ-index eastern box region). Given this zonal and inter-model variability, we adopted two complementary strategies for the BJ index diagnostic framework.

Strategy 1 (Constant MLD): A fixed MLD of a constant value is applied to both f3-L and f3-H when computing the BJ index. This approach follows the conventional practice in previous BJ index studies (e.g., Kim and Jin, 2011a, 2011b; Chen et al., 2019a, 2019b) and facilitates a direct comparison between the two simulations under an identical diagnostic framework. From the perspective of the BJ-index eastern-box average, the climatological mean MLD over the eastern equatorial Pacific is approximately 65 m in f3-L and 50 m in f3-H. Therefore, in this first approach, we use a constant value of 65 m for both simulations.

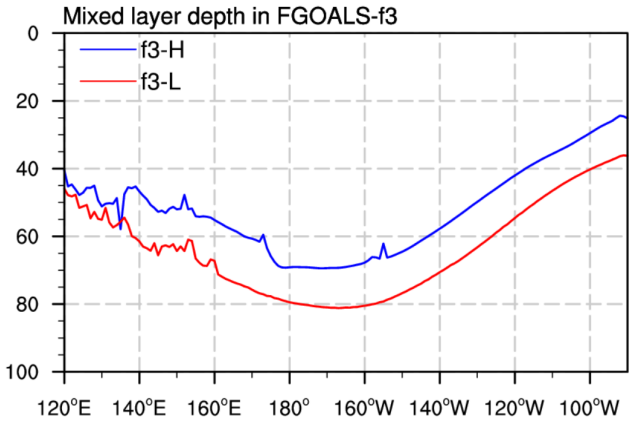

Figure B1. The longitudinally varying climatological mixed layer depth (unit: m) averaged over the equatorial Pacific (5°S–5°N) in f3-L (red line) and f3-H (blue line).

The BJ index results under Strategy 1 are shown in Figure B2. Figure B2 presents the BJ index calculated using a fixed MLD for the reanalysis, f3-L, and f3-H, as well as their difference (f3-L minus f3-H). The results demonstrate that although both models yield negative BJ indices, the value for f3-L is significantly larger (i.e., less negative) than that for f3-H. According to the physical interpretation of the BJ index (Jin et al., 2006; Kim and Jin, 2011a; 2011b), the less negative BJ index in f3-L indicates that the coupled air-sea system in f3-L is more unstable than that in f3-H. This more unstable coupled system is more favorable for ENSO growth, thereby leading to a stronger ENSO amplitude in f3-L than that in f3-H.

It is worth noting that the BJ index derived from ORAS5 is not more negative than that of f3-L, despite the observed ENSO amplitude being smaller than that simulated by f3-L. This apparent inconsistency can be attributed to two factors. First, reanalysis products carry inherent uncertainties, and direct comparison between reanalysis-derived and model-derived BJ indices should be interpreted with caution. Second, the BJ index is a linear diagnostic framework that does not account for nonlinear processes, including nonlinear atmospheric responses, semi-stochastic atmospheric noise (i.e., the high-frequency zonal wind anomalies discussed in this study), and oceanic nonlinear processes such as nonlinear dynamical heating. In other words, while the BJ index is a useful tool for assessing whether the linear air–sea coupling framework favors ENSO growth, the actual ENSO amplitude is jointly determined by linear coupling, nonlinear processes, and stochastic forcing. This represents an inherent limitation of the BJ index framework. Therefore, a comprehensive evaluation of ENSO simulation requires not only the BJ index analysis of linear feedback processes but also diagnostics beyond the linear framework to assess the roles of nonlinear processes and stochastic forcing—as is addressed in Section 5 of this study. In the following, our primary focus is on

examining the differences in the BJ index and its contributing terms between f3-L and f3-H.

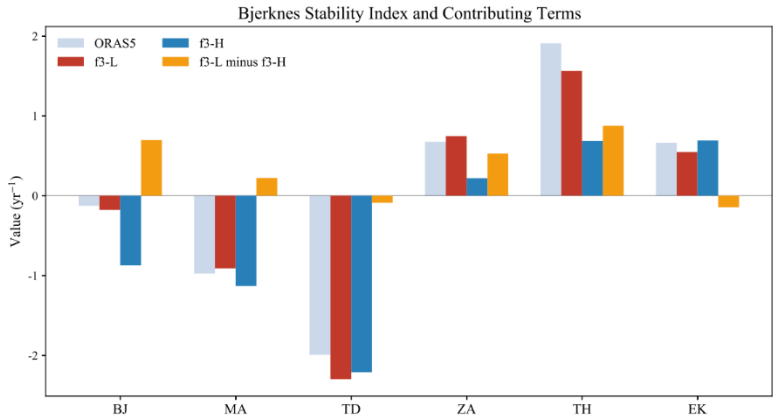

Figure B2. BJ index and the corresponding main contributing terms for the reanalysis (grey bars; ORAS-5), f3-L (red bars), f3-H (blue bars) and their difference (f3-L minus f3-H, orange bars). The BJ index is calculated using a fixed MLD of 65 m. The five contributing terms include dynamic damping by mean advection (MA), thermodynamic damping feedback (TD), zonal advection feedback (ZA), thermocline feedback (TH) and Ekman feedback (EK).

A further question arises: which physical processes contribute to the more unstable coupled system in f3-L? By examining the differences in the five contributing terms of the BJ index (orange bars in Fig. B2), we find that the thermocline feedback (TH) term and the zonal advection feedback (ZA) term are the decisive factors driving the BJ index difference between the two model versions. Therefore, the subsequent analysis focuses on the physical mechanisms responsible for the stronger TH and ZA terms in f3-L relative to f3-H.

Strategy 2 (Longitude-varying MLD): Each model version uses its own longitude-dependent climatological MLD (averaged over the equatorial band, 5°S–5°N) when computing the BJ index. This approach accounts for zonal variations and inter-model differences in stratification, providing a more physically realistic diagnostic. In this approach, when calculating the BJ index, we diagnose the mixed-layer temperature anomaly above the longitudinally varying climatological mixed layer depth (Figure B1) within the three-dimensional eastern equatorial Pacific box.

Figure B3 presents the BJ index and its contributing terms calculated using the longitude-varying MLD for the reanalysis, f3-L, and f3-H, as well as their difference (f3-L minus f3-H). The main results are broadly consistent with those obtained under Strategy 1. Specifically, the BJ index of f3-H remains more negative than that of f3-L, which largely explains the weaker ENSO amplitude in f3-H; and the BJ index difference between the two models is still primarily attributable to the TH and ZA terms.

The only notable discrepancy between the two strategies lies in the mean advection (MA) term, which represents the dynamic damping by mean zonal and meridional advection. Under Strategy 2, the MA term exhibits a considerably larger difference between f3-L and f3-H than under Strategy 1. To understand this, we further decomposed the MA term into its two components: the damping by mean zonal current (R1 = $-a_1 \frac{\langle \Delta \bar{u} \rangle_E}{L_x}$) and the damping by mean meridional current (R2 = $-a_2 \frac{\langle \Delta \bar{v} \rangle_E}{L_y}$). As shown in Figure B4, the MA term difference primarily arises from the meridional component (R2).

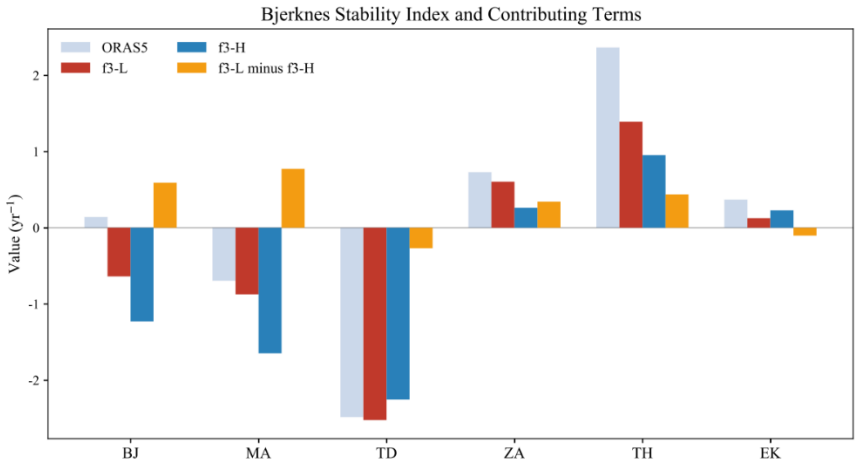

Figure B3. Same as Figure B2, but the BJ index is calculated using the longitude-varying MLD.

This meridional damping component is closely related to the mean subtropical cell (STC) circulation in the central-eastern equatorial Pacific. Figure B5 shows the latitude–depth distribution of the mean ocean currents and ENSO-related ocean temperature anomalies averaged over 150°W–90°W. The ENSO-related temperature anomalies are centered at the equator from the surface down to approximately 100 m, and are advected poleward by the mean meridional currents, constituting a dynamical damping effect. In both models, the mean meridional flow associated with the STC is directed poleward above approximately 40 m but equatorward below 40 m. Consequently, the advection of temperature anomalies by the mean meridional current reverses sign at approximately 40 m, so that the contributions from the upper and lower portions partially cancel each other. When a constant MLD of 65 m is used for vertical averaging, this cancellation occurs similarly in both models, yielding comparable MA terms. However, under the longitude-varying MLD strategy, the shallower MLD in f3-H means that the vertical averaging captures a thinner layer in which the poleward (damping) branch dominates, resulting in a more negative MA term in f3-H compared

to f3-L. This MLD sensitivity of the MA term partially explains why the BJ index in f3-H becomes even more negative under Strategy 2.

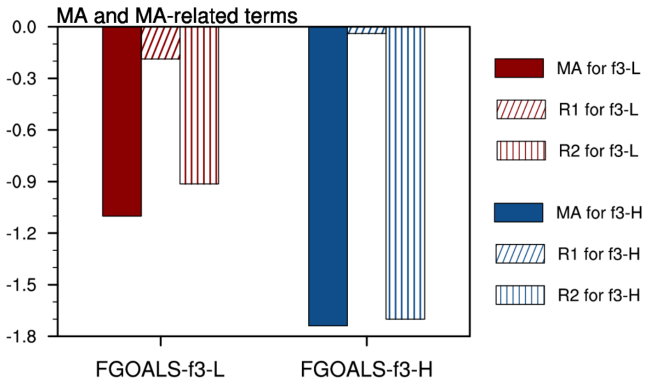

Figure B4. The MA term and its two components: dynamic damping by mean zonal current (R1 = $-a_1 \frac{\langle \Delta \bar{u} \rangle_E}{L_x}$) and dynamic damping by mean meridional current (R2 = $-a_2 \frac{\langle \Delta \bar{v} \rangle_E}{L_y}$), for f3-L (red) and f3-H (blue).

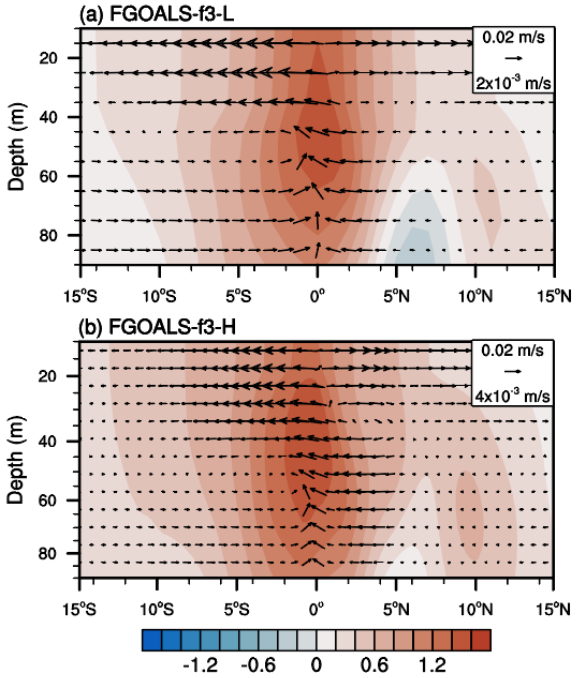

Figure B5. Oceanic mean currents (vectors, units: m s^{-1}) and ENSO-related ocean temperature anomalies (contours, units: °C) averaged over 150°W–90°W for (a) f3-L and (b) f3-H. Here the ENSO-related ocean temperature anomalies are obtained by regressing the ocean temperature anomaly field onto the Niño3.4 index.

In summary, the sensitivity test demonstrates that the core conclusions of the BJ index analysis, that is namely, the more unstable coupled system in f3-L and the dominant roles of the TH and ZA terms are robust across both MLD strategies.

Jin, F. F., Kim, S. T., and Bejarano, L.: A coupled-stability index for ENSO,

Geophysical Research Letters, 33, https://doi.org/10.1029/2006gl027221, 2006.

Wang, L., Li, T., and Zhou, T. J.: Intraseasonal SST variabil-ity and air-sea interaction over the Kuroshio extension region during boreal summer. Journal of Climate, 25, 1619–1634, https://doi.org/10.1175/JCLI-D-11-00109.1, 2012.

Chen, L., Li, T., Behera, S. K., and Doi, T.: Distinctive precursory air–sea signals between regular and super El Niños, Advances in Atmospheric Sciences, 33, 996–1004, https://doi.org/10.1007/s00376-016-5250-8, 2016.

Kim, S. T. and Jin, F.-F.: An ENSO stability analysis. Part II: Results from the twentieth and twenty-first century simulations of the CMIP3 models, Climate Dynamics, 36, 1609–1627, https://doi.org/10.1007/s00382-010-0872-5, 2011a.

Kim, S. T. and Jin, F.-F.: An ENSO stability analysis. Part I: results from a hybrid coupled model, Climate Dynamics, 36, 1593–1607, https://doi.org/10.1007/s00382-010-0796-0, 2011b.Chen, L., Wang, L., Li, T., and Liu, J.: Drivers of reduced ENSO variability in mid-Holocene in a coupled model, Climate Dynamics, 52, 5999–6014, https://doi.org/10.1007/s00382-018-4496-5, 2019a.

Chen, L., Zheng, W., and Braconnot, P.: Towards understanding the suppressed ENSO activity during mid-Holocene in PMIP2 and PMIP3 simulations, Climdate Dynamics, 53, 1095-1110, https://doi.org/10.1007/s00382-019-04637-z, 2019b.

3. The comparison between the CMIP experiments and the OMIP experiments is interesting. However, it seems that the response of thermocline depth anomalies to zonal wind stress differs between OMIP and CMIP in a resolution-dependent manner (i.e., OMIP shows a stronger response than CMIP at high resolution, but a weaker response at low resolution). What are the physical reasons for this contrasting behavior?

Reply: We thank the reviewer for this excellent and insightful comment. We fully agree that the resolution-dependent contrast between the OMIP experiment and the CMIP experiment (i.e., the historical experiment) is a noteworthy phenomenon that warrants explanation. We have carefully analyzed the physical reasons behind this behavior, and our findings are summarized as follows:

As established in Section 4.2, equatorial thermocline depth anomalies are primarily driven by surface wind stress forcing, and the meridional structure of the zonal wind stress anomalies (τ_x') plays a critical role in determining the efficiency of this forcing.

To understand the contrasting OMIP–CMIP behavior, we compared the meridional structures of the "normalized τ_x'" between the CMIP and OMIP experiments for both model versions, as shown in Figure B6. Here the normalized τ_x' is obtained by regressing the τ_x' field onto Nino4-region-averaged τ_x'; and then averaging over the Nino4 longitude range (160°E–150°W). This normalization procedure enables a fair comparison of the meridional structure of τ_x' across different experiments and model versions. In f3-L, the CMIP experiment produces stronger τ_x' near the equator compared to the OMIP forcing, which is derived from the JRA55-do reanalysis (red lines in Fig. B6). This leads to an enhanced thermocline response in CMIP relative to OMIP. Conversely, in f3-H, the CMIP experiment yields weaker equatorial τ_x' than the OMIP forcing (blue lines in Fig. B6), resulting in a weaker thermocline response in CMIP relative to OMIP. This explains the resolution-dependent contrast identified by the reviewer.

To further quantify these structural differences in τ_x' between the CMIP and OMIP experiments, the meridional distribution index (*MDI*) that was proposed by Chen et al. (2015), is employed. The MDI is defined as:

$$MDI = \frac{\int_{-10^\circ}^{10^\circ} \tau_x'(y)|y|dy}{\int_{-10^\circ}^{10^\circ} \tau_x'(y)dy} \quad (7)$$

where y denotes latitude, and τ_x'(y) represents the meridional profile of the normalized τ_x' shown in Fig. B6. The *MDI* provides a quantitative measure of the meridional concentration of ENSO-related τ_x' within the equatorial band. Specifically, a smaller MDI indicates that τ_x' is more concentrated near the equator, whereas a larger MDI indicates a broader meridional distribution.

The qualitative differences in τ_x' distributions shown in Fig. B6 are corroborated by the MDI results (Table B1). In f3-L, the CMIP experiment yields a notably smaller MDI (2.55°) than the OMIP experiment (2.68°), indicating a more equatorially concentrated τ_x' structure that can more efficiently drive thermocline variability, and hence produces a larger β_h in the CMIP experiment. Conversely, in f3-H, the CMIP experiment exhibits a larger MDI (2.71°) than the OMIP experiment (2.64°), corresponding to a broader τ_x' distribution that drives a more moderate thermocline response and a smaller β_h.

In summary, this resolution-dependent contrast between the CMIP and OMIP experiments further reinforces our core conclusion: the meridional structure of τ_x', particularly its degree of equatorial concentration, is the primary factor governing the

strength of the thermocline feedback. These results also highlight the sensitivity of ENSO-related air-sea coupling to even subtle differences in equatorial wind stress meridional distribution: a small resolution-induced change in the meridional structure of τ_x' can produce substantially different thermocline responses, which in turn fundamentally modulate the associated air-sea coupling processes. Consequently, an accurate representation of the wind stress meridional structure is critical for improving ENSO simulations in climate models. To respond to this concern, we have incorporated the relevant analysis and the corresponding results into the revised manuscript.

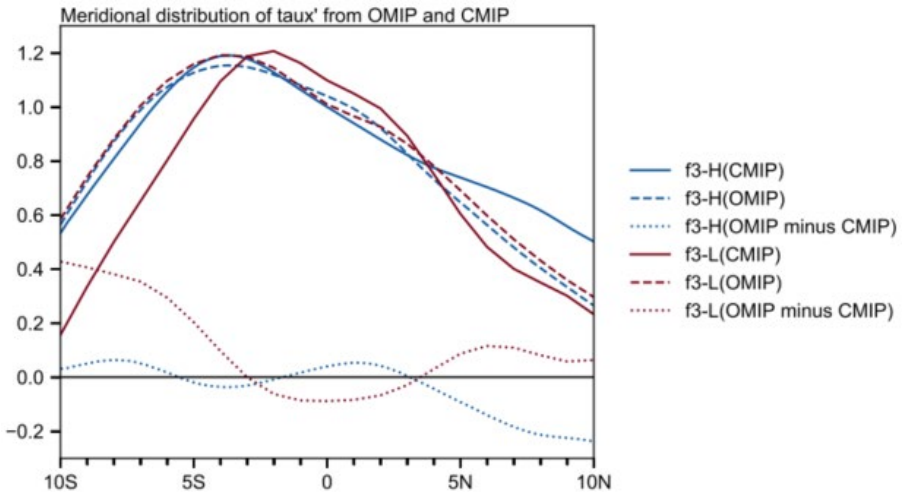

Figure B6. Meridional structure of normalized zonal wind stress anomalies [units: N m^{-2} (N m^{-2})$^{-1}$] averaged over 160°E–150°W for f3-L in CMIP (red solid line), f3-L in OMIP (red dashed line), and their difference (red dotted line, OMIP minus CMIP); f3-H in CMIP (blue solid line), f3-H in OMIP (blue dashed line), and their difference (blue dotted line, OMIP minus CMIP). The normalized zonal wind stress anomalies are obtained by regressing the zonal wind stress anomaly field onto the Niño4 region (5°S–5°N, 160°E–150°W) averaged zonal wind stress anomalies and then averaged over the Nino4 longitude range (160°E–150°W).

Table B1. Meridional distribution index (MDI; units: °) of τ_x', calculated from the meridional structure of normalized τ_x' as shown in Fig. B6.

	f3-L	**f3-H**
CMIP	2.55	2.71
OMIP	2.68	2.64

Chen, L., Li, T., and Yu, Y. Q.: Causes of strengthening and weakening of ENSO amplitude under global warming in four CMIP5 models, Journal of Climate, 28, 3250–3274, https://doi.org/10.1175/jcli-d-14-00439.1, 2015.

4. The BJ index provides a useful linear stability framework for interpreting ENSO amplitude changes. However, given the relatively limited simulation length (~65 years)

and the analysis being based on a single model family, it would be helpful for the authors to briefly acknowledge the potential limitations of applying a linear BJ framework to interpret resolution-dependent changes in ENSO dynamics in the discussion, particularly considering the role of nonlinear and stochastic processes.

Reply: We thank the reviewer for this thoughtful suggestion. We fully agree that the limitations of the linear BJ framework should be explicitly acknowledged, particularly in the context of resolution-dependent ENSO dynamics.

In fact, as discussed in our response to Comment 2, we have already added a dedicated discussion of this issue in the revised manuscript (Section 4.1). Specifically, we note that the BJ index is a linear diagnostic framework that does not account for nonlinear processes, including nonlinear atmospheric responses, semi-stochastic atmospheric noise (i.e., the high-frequency zonal wind anomalies discussed in Section 5), and oceanic nonlinear processes such as nonlinear dynamical heating (Wei et al., 2026). While the BJ index is a useful tool for assessing whether the linear air–sea coupling framework favors ENSO growth, the actual ENSO amplitude is jointly determined by linear coupling, nonlinear processes, and stochastic forcing. Therefore, a comprehensive evaluation of ENSO simulation requires not only the BJ index analysis of linear feedback processes but also diagnostics beyond the linear framework—as is addressed in Section 5, where we examine the role of high-frequency stochastic wind forcing in shaping ENSO irregularity.

Regarding the relatively limited simulation length (~ 65 years), we acknowledge that this may induce sampling uncertainty in the BJ index estimates. However, the historical experiment of f3-H (highresSST-present) only provides simulation outputs covering 1950–2014, which is comparable to the analysis periods adopted in previous BJ index studies (e.g., Kim and Jin, 2011a, 2011b).

We have incorporated some relevant discussions into the revised manuscript to explicitly acknowledge these limitations. We thank the reviewer for helping us strengthen this aspect of the paper.

Kim, S. T. and Jin, F.-F.: An ENSO stability analysis. Part II: Results from the twentieth and twenty-first century simulations of the CMIP3 models, Climate Dynamics, 36, 1609–1627, https://doi.org/10.1007/s00382-010-0872-5, 2011a.

Kim, S. T. and Jin, F.-F.: An ENSO stability analysis. Part I: results from a hybrid coupled model, Climate Dynamics, 36, 1593–1607, https://doi.org/10.1007/s00382-010-0796-0, 2011b.

Wei, X. J. Chen, L., and Sun, M.: Fine-tuning Atmospheric Parameters for Improving ENSO Simulation in the Zebiak–Cane Model, Advances in Atmospheric Science, 43, 420–435, https://doi.org/10.1007/s00376-025-4423-8, 2026.

5. In Figure 7a, there seems to be a horizontal black line around 0.2, but it is not described in the caption. Please clarify what this line represents.

Reply: We thank the reviewer for pointing this out. We apologize for the confusion. The horizontal black line at 0.2 in the original Figure 7a was added solely as a visual guide to separate the difference curve (orange dashed line) from the individual model curves (red and blue solid lines) and does not represent any physical threshold. In the revised manuscript, we have removed this line and replaced it with a horizontal reference line at 0.0, which serves as baseline for assessing the sign of the resolution-induced differences. For the reviewer's convenience, the updated plot is copied below.

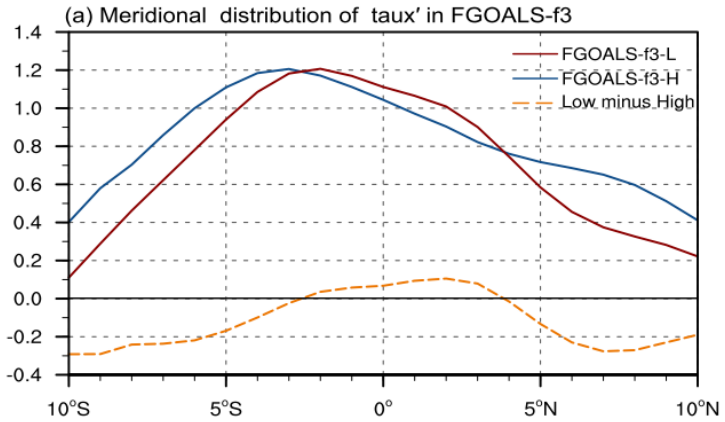

Figure B7. Meridional structure of normalized zonal wind stress anomalies [units: N m^{-2} (N m^{-2})$^{-1}$] averaged over the Niño4 longitude range (160°E–150°W) for f3-L (red solid line), f3-H (blue solid line) and their difference (orange dash line, f3-L minus f3-H). In this plot, all the data are interpolated onto a 1° x 1° grid to facilitate the comparison.

6. Lines 29-30. The sentence "The low-resolution severely overestimates ENSO amplitude" lacks a noun after "low-resolution." Please revise (e.g., "low-resolution version").

Reply: Corrected as suggested.

7. Line 38: The word "feeble" sounds somewhat informal in this context. Please consider replacing it with "weak".

Reply: Done as suggested.

8. Line 422: “may be not the primary driver” contains a word order issue. Please revise to “may not be the primary driver.”

Reply: Corrected as suggested.

9. Line 500: “yielding a more realistic characteristics of TC activity” contains a number agreement issue. Please revise to either “yielding more realistic characteristics of TC activity” or “yielding a more realistic representation of TC activity.”

Reply: Corrected as suggested.